Converted-wave processing and interpretation at Cold Lake, Alberta

J. Helen Isaac and Don. C. Lawton

ABSTRACT

Two experimental time-lapse converted-wave surveys were acquired by Imperial Oil Resources Ltd. at Cold Lake, Alberta, where bitumen is produced from the Clearwater Formation by means of cyclical steam stimulation of the reservoir. The survey consisted of seven source lines and one common receiver line. The *P-P* and *P-S* data from three common CDP/CCP lines were processed fully for each survey. The *P-S* data processing flow included post-NMO spiking deconvolution, *f-k* filtering and spectral balancing to enhance the important reflections and boost the higher frequencies. Each pair of *P-P* and *P-S* lines was interpreted on a workstation and *Vp/Vs* ratios were calculated from the Grand Rapids to Devonian interval transit times. Values of *Vp/Vs* over the steamed zone ranged from 2.01 to 2.20 and over the cold reservoir averaged 2.20, which is in agreement with the theoretical values. In general, there is a good correlation between low *Vp/Vs* ratios (below 2.1) and the locations of steam injection wells.

INTRODUCTION

At Cold Lake, Alberta, Imperial Oil Resources Ltd. is producing bitumen from the Lower Mannville Clearwater Formation sands by means of cyclical steam stimulation of the reservoir. In the area of this study, steam is injected into the reservoir at a temperature of 280˚C and at a fluid pressure of 6-7 MPa. Experimental studies on heavy oil- and bitumen-saturated sands indicate that a significant decrease in compressional wave velocity should result during steaming because of the conditions of high temperature and low effective pressure (e.g., Tosaya et al., 1987; Wang and Nur, 1988a and b). Eastwood (1993) documented experimental and theoretical modelling studies on the Cold Lake oil sands from this study area. His work predicts a very large drop in compressional wave velocity (*Vp*) over a temperature rise from 20˚C to 200˚C while only a very small increase in shear wave velocity (*Vs*) is predicted over the same temperature range. During the production cycle the *P*-wave interval velocity decreases due to the presence of gas-saturated zones. These results suggest that determination of *Vp/Vs* or Poisson's ratios over a steamed reservoir may provide additional information about lateral and temporal changes in reservoir conditions.

Imperial Oil acquired two experimental time-lapse converted-wave seismic surveys over a producing pad at Cold Lake. The first survey was acquired in November 1993 at the peak of the steaming cycle while the follow-up survey was acquired in April 1994 during the production cycle. Each converted-wave survey was part of a 3-D *P-P* survey and the acquisition geometry was identical. The compressional source for the 3-D survey was used and both reflected compressional and mode-converted shear energy were recorded by three-component geophones at the surface. It was hoped that *Vp/Vs* ratios could be obtained from the data and related to the reservoir conditions at the times of acquisition of the data.

The layout of the survey is shown in Figure 1. One receiver line of three-component geophones was laid out on the surface to coincide with a source line (line

470) and these geophones recorded data from the shots along seven source lines in the 3-D survey. The source and receiver station interval was 16 m and the source lines spaced 125 m apart. The receiver line and source lines 468 to 473 were 1800 m long, (114 stations each) and line 474 was 750 m (48 stations). The source was 0.125 kg of dynamite buried 12 m deep and a total of 732 live shots was recorded. Each record of 342 traces was separated into three components: one vertical (*P-P)* and two horizontal (*P-S*). Processing of the *P-P* data and preliminary processing of the *P-S* data were discussed in the CREWES Research Report Volume 6 (Isaac and Lawton, 1994). In this paper, the full *P-S* processing flow is described, followed by preliminary data interpretation.

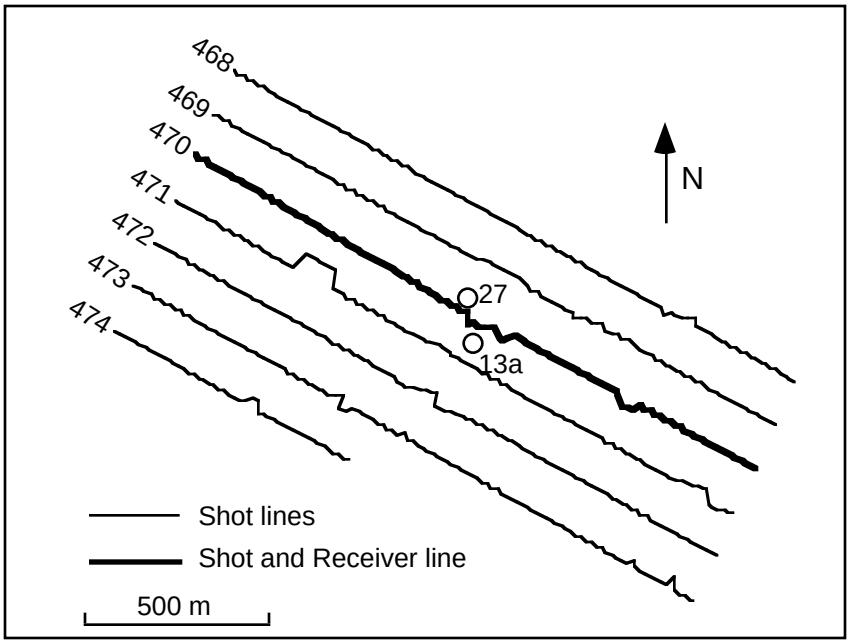

Fig. 1. Layout of the converted-wave survey.

P-S PROCESSING

Three lines each of *P-P* and *P-S* records were processed fully. Line 470 is the line of coincident sources and receivers so both components were processed for this line. The common conversion point (CCP) bins for the *P-S* component of lines 468 and 472 corresponded to the CDP bins for the *P-P* components of lines 469 and 471, respectively. Thus the *P-P* lines fully processed were 469, 470 and 471 while the *P-S* lines fully processed were 468, 470 and 472. Vertical lines 468 and 472 were partially processed to determine the shot statics solutions for those lines.

The processing flow is shown in Figure 2. Rotation analysis to determine the natural coordinate system was inconclusive so each pair of horizontal records was rotated only into components oriented in the source-receiver plane and orthogonal to that plane. The data were binned using an asymptotic 3-D binning algorithm developed in the CREWES Project (Lane and Lawton, 1993) and *Vp/Vs* of 2.4. Determination of the *S*-wave statics solution was described previously (Isaac and Lawton, 1994).

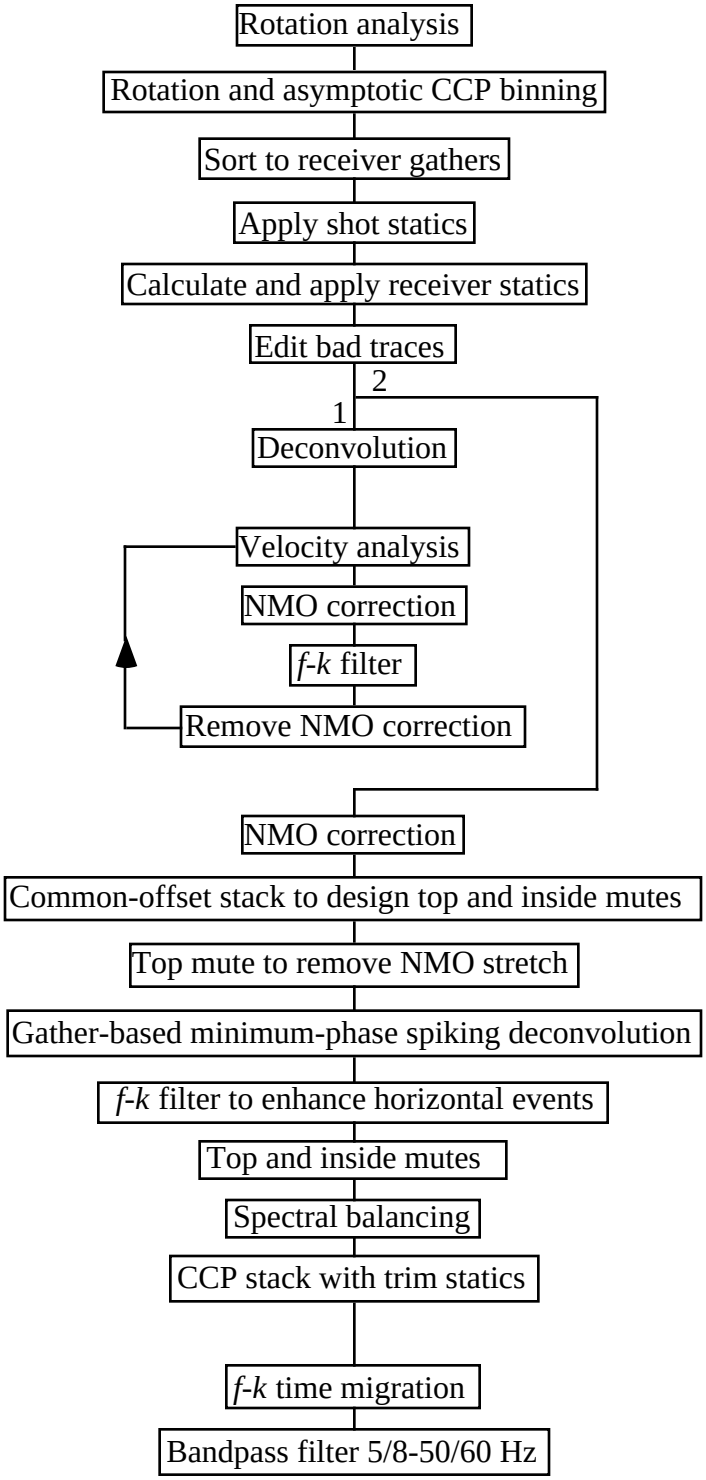

Fig. 2. Processing flow for the *P-S* data.

This statics solution is shown in Figure 3. Here it is seen clearly how large and variable are the *S*-wave statics compared to the *P*-wave statics. After application of the statics corrections, spiking deconvolution was applied to the receiver gathers and an iterative process used to determine the stacking velocities. The approximation of *P*-*S* moveout to hyperbolic is only valid at short offsets (Iverson, 1989) and, since the target zone is at a relatively shallow depth (less than 500 m), inclusion of the longer offsets may degrade the velocity analysis. NMO velocities estimated from semblance analyses were applied to the data, the gathers *f*-*k* filtered to eliminate events with high dip (primarily the *P*-*P* energy), NMO reapplied and velocity analysis repeated.

This sequence was repeated a few times to establish the optimum stacking velocities. These velocities proved difficult to determine because the data, especially in the shallower section above 0.6 s, were dominated by *P*-*P* energy. *P*-*P* energy contaminates the *P*-*S* data because the upcoming wave is not strictly vertical. Different stacking velocities were obtained from semblance analyses than from constant velocity stacks. The semblance analyses are considered to be more reliable because in their creation the NMO stretch mute can be controlled whereas in the constant velocity stacks it cannot. Reducing the data set to traces with shorter offsets did not help. The final velocities chosen were those which resulted in the best stacked section and were obtained from the semblance analyses. Representative stacking velocities are listed in Table 1.

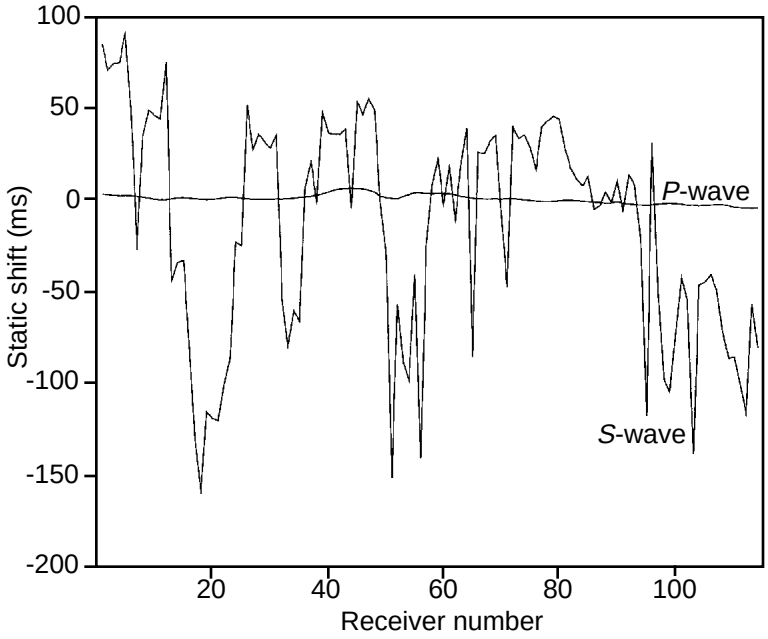

Fig. 3. *P*-wave and *S*-wave receiver statics solutions.

The resulting stacked section was not as good as anticipated, having lower bandwidth than was hoped for. It is possible that application after deconvolution of the NMO correction with the low velocities is causing a loss of higher frequencies. To overcome this, pre-stack deconvolution was applied after NMO correction instead of before. Spectral balancing was also applied at this stage. This improved greatly the frequency content and continuity of reflectors in the final stacked section. The NMO-corrected, deconvolved shot gathers were then *f*-*k* filtered to remove the *P*-*P*

energy that was degrading them. Common-offset stacks were used to determine the inside and top mutes to be applied to the NMO-corrected, deconvolved, *f-k* filtered gathers. The inside mute cut out any residual shot noise. The top mute was applied prior to *f-k* filtering to remove NMO stretch and after *f-k* filtering to eliminate edge effects and to limit the farthest offset to 1400 m.

Table 1. Representative *P-S* stacking velocities for line 470.

Time (s)	**V*p-s* (m/s)**
0.100	930
0.200	970
0.300	1020
0.400	1060
0.500	1120
0.700	1200
0.800	1260
1.200	1425
1.400	1500

In Figure 4 are plotted the top and inside mute offsets as a function of depth. The dashed area denotes the range of offsets included at any depth. On average, at any depth, the ratio of the farthest offset to depth is 1.4 and of the nearest offset to depth is 0.5. The longest source-receiver offset on the three processed lines was 1810 m but offsets greater than 1390 m were excluded from the stack. A deleterious effect of limiting the offsets included in any CCP gather is to reduce the fold of the data. Figure 5 shows the final fold of line 470-94 at a) each CDP along the *P-P* section and at b) each CCP along the *P-S* section. O denotes the original fold after binning while D and GR denote the fold at the tops of the Devonian section and Grand Rapids Formation, respectively, after muting. The plots of fold are not symmetrical because of asymmetry in the line geometry (see Figure 1) and exclusion of bad shots. Average fold over CDPs 20 to 200 on the *P-P* section is 40 at the top Devonian level and 27 at the top Grand Rapids level. In comparison, for the *P-S* section, fold over CCPs 20 to 200 is 22 at the top Devonian level and 16 at the top Grand Rapids level. Due to an unusually large number of bad shots and poor record quality along line 472-93, there were no data at the top Grand Rapids level over CCPs 97 to 114.

Spectral balancing was applied to the NMO-corrected, deconvolved gathers before stacking to boost frequencies up to 60 Hz. In Figure 6 are shown the spectra of raw records from the a) *P-P* and b) *P-S* gathers and the spectra of the final stacked section from the c) *P-P* and d) *P-S* data of line 470. The raw *P-P* record has a dominant frequency of 40 Hz while that of the *P-S* record is down at 15 Hz. After deconvolution the individual spectra are much better balanced. On the *P-S* records it

was found that an upper frequency limit of about 60 Hz enhanced visibly the Devonian reflector on the final stacked section. The dominant frequencies of about 60 Hz in the *P-P* data and 30 Hz in the *P-S* data result in comparable wavelengths of 35 to 40 m in the reservoir zone.

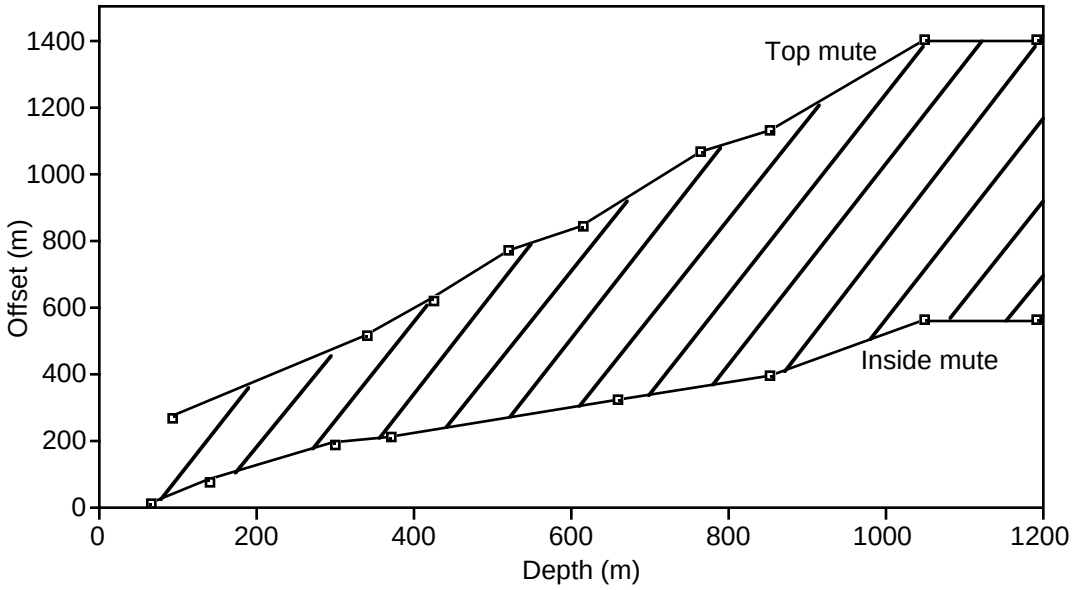

Fig. 4. Range of offsets included in the *P-S* gathers.

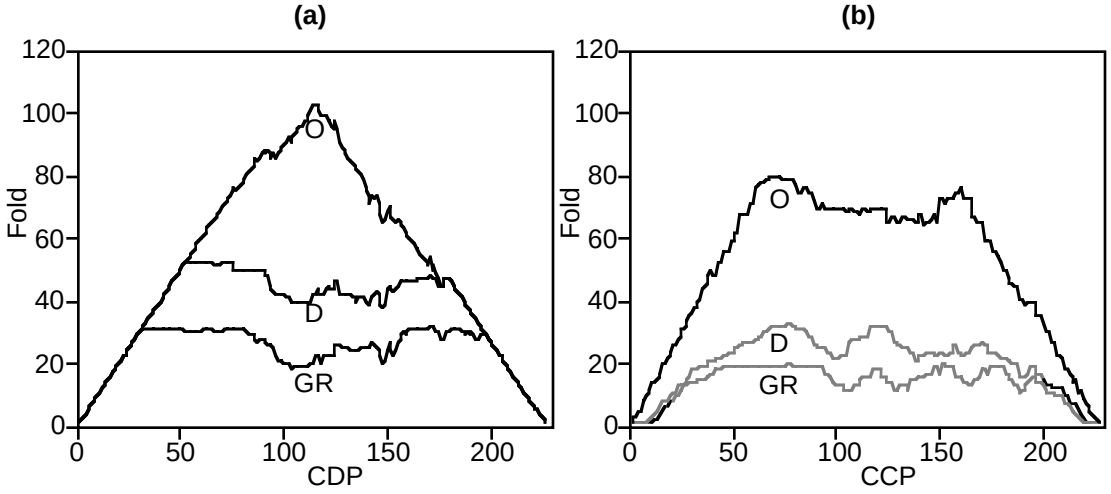

Fig. 5. The results on the final stack fold of muting and limiting the offsets for a) the *P-P* data and b) the *P-S* data. O denotes the original fold, D the fold at the Devonian level and GR the fold at the Grand Rapids level.

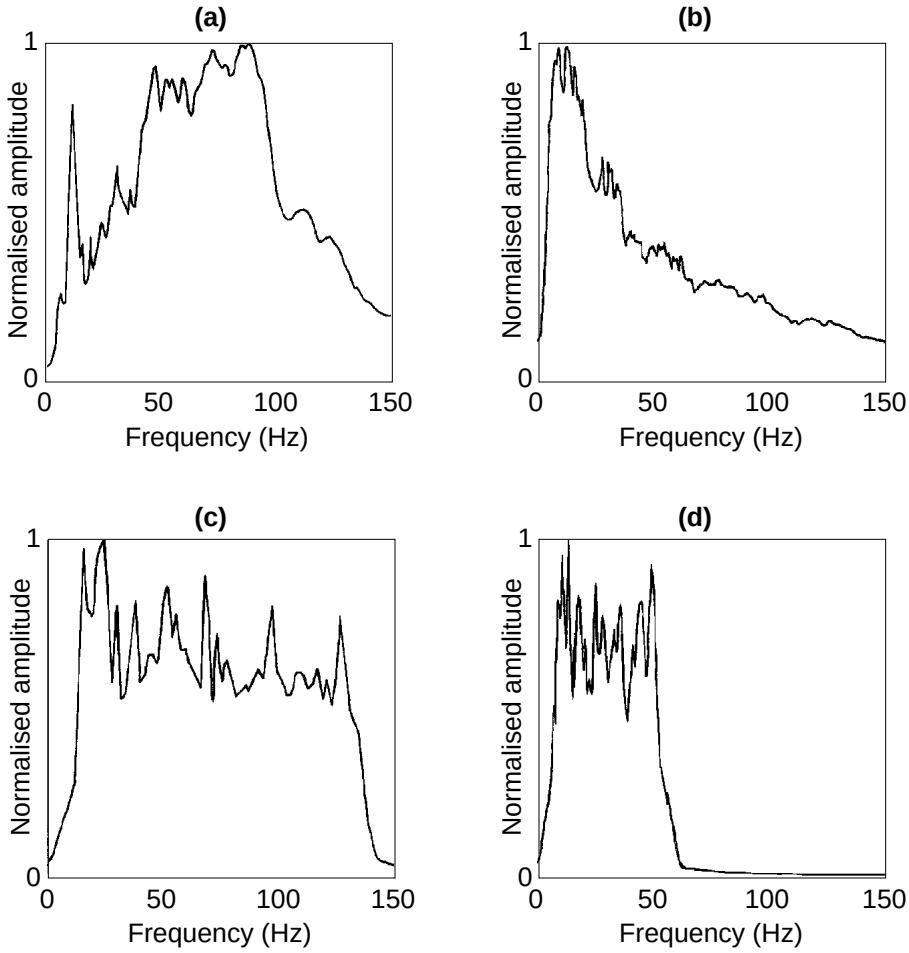

Fig. 6. Amplitude spectra for a) a raw *P-P* record, b) a raw *P-S* record, c) final stacked *P-P* section and d) final stacked *P-S* section.

Harrison and Stewart (1993) migrated *P-S* sections using post-stack phase-shift time-migration with migration velocities 6-11% less than the *P-S* rms velocities. The three *P-S* lines from each survey were post-stack time-migrated using *f-k* migration and a bandpass filter of 5/8 - 50/60 Hz was applied to the sections. Finally, an *f-x* deconvolution was applied to the migrated section to enhance reflectors. The final migrated *P-S* section for line 470-93 is shown in Figure 7. The scarcity of signal in the shallower section is due to the dominance of *P*-wave energy there and the degradation of data outside the trim statics window. In Figure 7 a strong event is visible at about 0.85 s; an event which was not resolved on the initial stacked section. This event was not apparent until the receiver statics had been calculated, deconvolution applied after NMO correction and the best stacking velocities had been obtained. The combination of these three factors resulted in a much improved section with interpretable events.

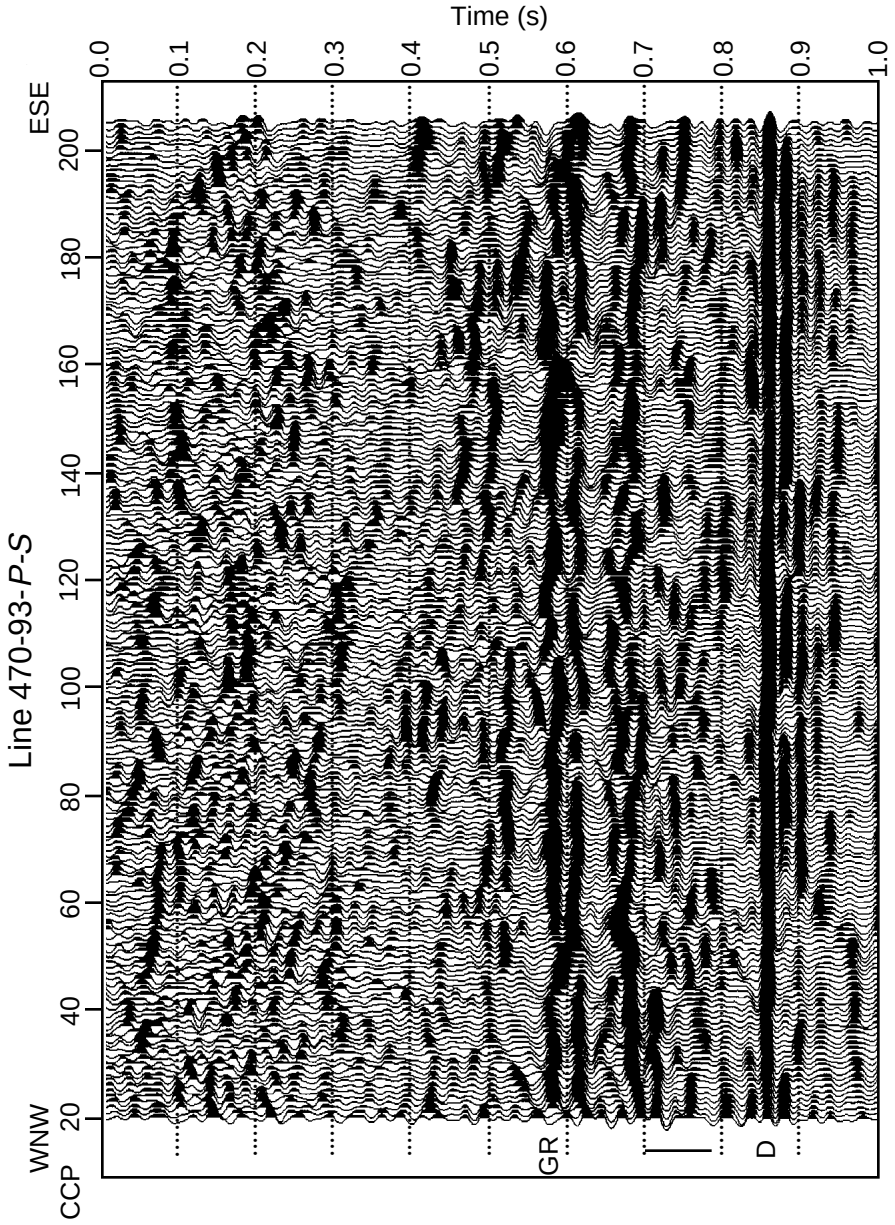

Fig. 7. Final migrated *P-S* line 470-93.

DATA INTERPRETATION

Vp/Vs ratios along a seismic line can be calculated from the interval transit times measured on corresponding *P-P* and *P-S* sections by using the following formula:

$$Vp/Vs = (2ts/tp) - 1 \quad (1)$$

where ts and tp denote the interval transit times as measured on the *P-P* and *P-S* sections, respectively. For equation (1) to be valid, it is critical that the depth intervals corresponding to these interval transit times are identical on both sections (Iverson et al., 1989). Not all interfaces produce good reflections on both the *P-P* and *P-S* sections, so care must be taken to select appropriate interfaces. The locations of the interpreted lines and the injection and production wells are shown in Figure 8.

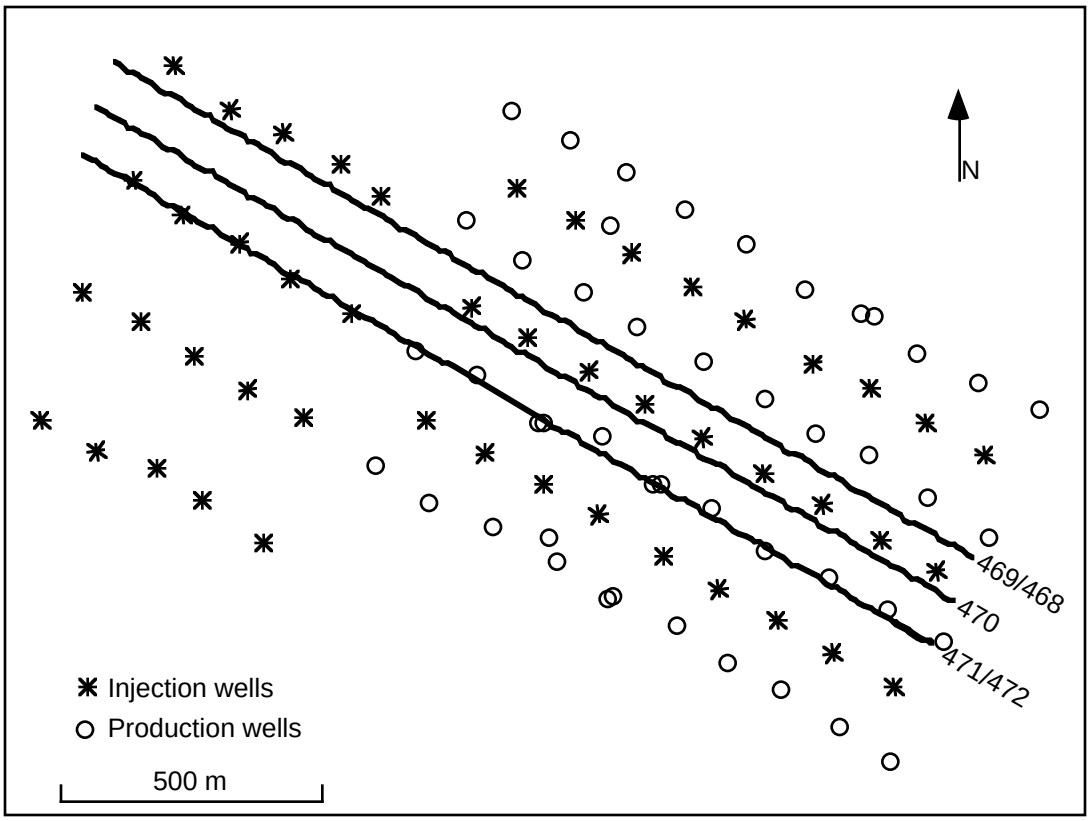

Fig. 8. Locations of the interpreted lines, injection and production wells.

Figure 9 shows the compressional and shear wave velocities as measured by dipole logs in well 13a and the corresponding *Vp/Vs* for each depth. A clear increase in velocity is observed for both the *P* and *S* curves at 315 m; the top of the Grand Rapids Formation. A good seismic reflection should therefore be expected for the Grand Rapids top on both the *P-P* and *P-S* sections. Between the top of the Grand Rapids and the Clearwater Formation at 416 m, there are no significant velocity contrasts on either curve. Unfortunately, the well penetrated no deeper than the Clearwater Formation so direct velocity measurements of the Devonian section are unavailable.

From a well log in the nearby D3 pad and 3-D velocity analysis it is known that the compressional wave velocity increases considerably at the top of the Devonian Formation. If it is assumed that *Vp/Vs* in carbonates is around 1.9, then the shear wave velocity can be expected to increase considerably, also. Therefore, the Devonian event is expected to be a strong, identifiable event on both the *P-P* and *P-S* sections.

The low *P*-wave velocity observed on the sonic log at the top of the Clearwater Formation is caused by a gas-saturated zone. *Vp/Vs* in this zone is anomalously low so measurement of such low values from the seismic data acquired during the production cycle should reflect gas-saturated zones. Differences in reflectivity between the *P-P* and *P-S* sections should also be apparent over such zones if the *P-S* data are of high enough resolution.

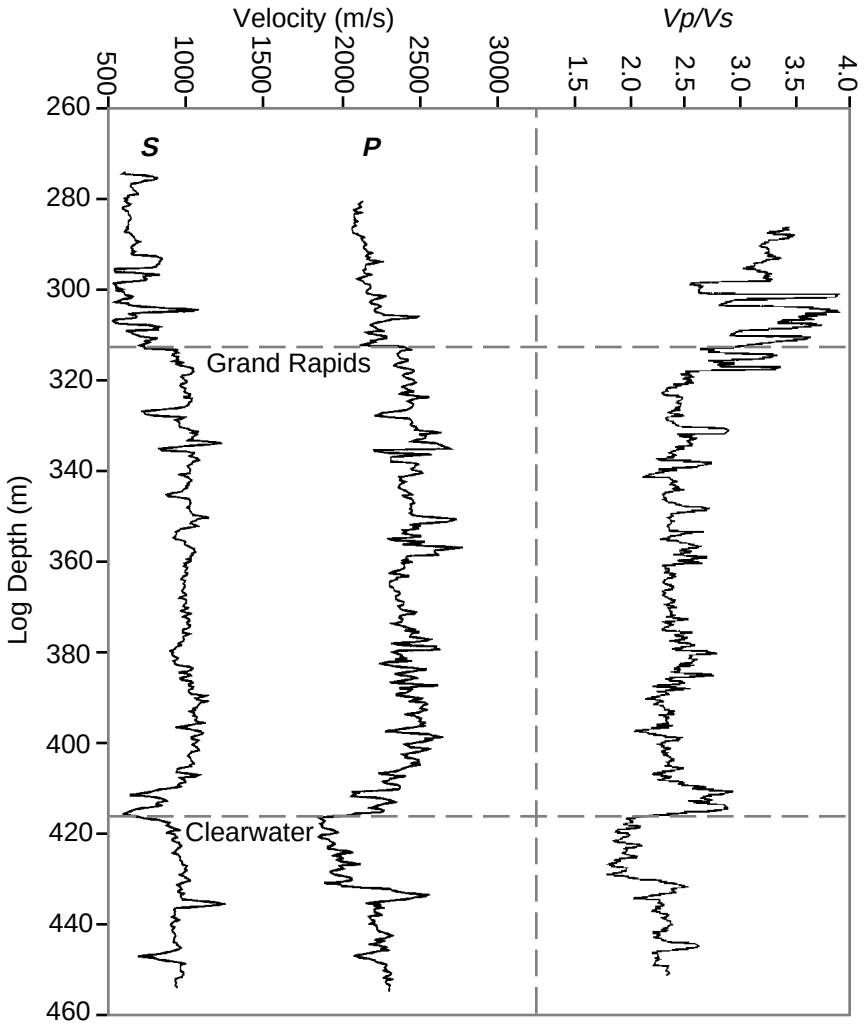

Fig. 9. Compressional and shear wave sonic velocities from a dipole log in well 13a and the corresponding *Vp/Vs* values.

A synthetic seismogram (*P-P*) was created using a sonic log from well 27 and the "SYNTH" program. In Figure 10 is shown the correlation between this seismogram and part of line 470-94-*P-P*. The sonic logs were acquired in February 1988 so there were several cycles of CSS between the times of acquisition of the sonic data and the seismic data. The character match between the synthetic seismogram allows for identification of the Grand Rapids and Clearwater Formation tops. Knowledge of the expected arrival times of the Clearwater and Devonian events, based on experience at the D3 pad, also helps to identify these events.

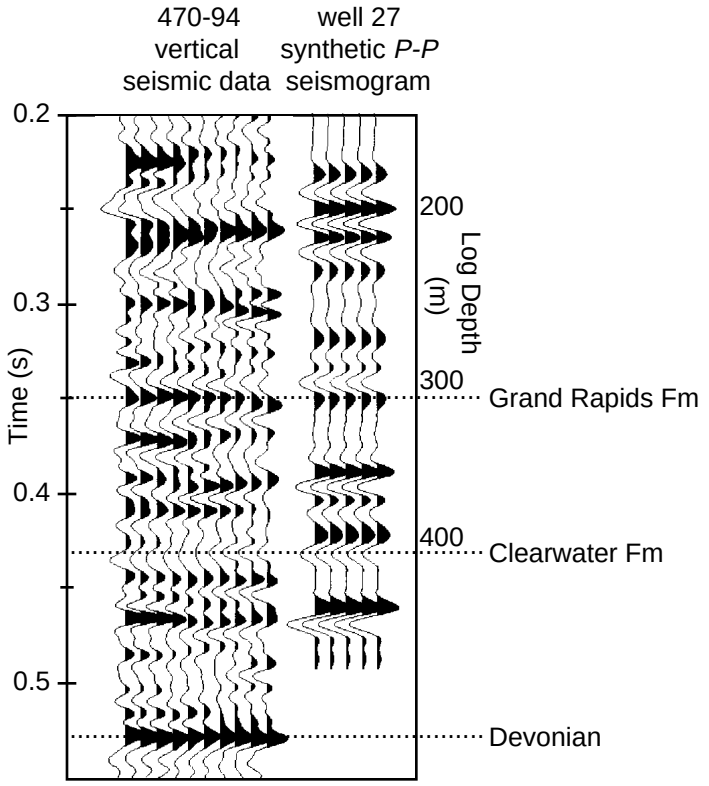

Fig. 10. Tie between *P-P* seismic data and *P-P* synthetic seismogram at well 27.

Interpreted versions of lines 470-93-*P-P* and 470-94-*P-P* are shown in Figures 11 and 12 respectively. The frequency content and seismic character appear to be similar. The tops of the Grand Rapids Formation at about 0.35 s and the Devonian section at 0.53 s are annotated on the sections. Indicated by the bar at the side of the sections is the Clearwater reservoir zone, which extends from about 0.43 to 0.47 s. The Grand Rapids and Devonian events were identified easily on the *P-P* migrated line 470 in Figures 11 and 12. Indicated on both of these sections is a channel shallow in the section. The location of the deepest part of the channel, over CDPs 25 to 49, corresponds to the location of receivers 13 to 25 in Figure 3, where the very high negative *S*-wave static values occur. This channel may be the cause of these large *S*-wave statics.

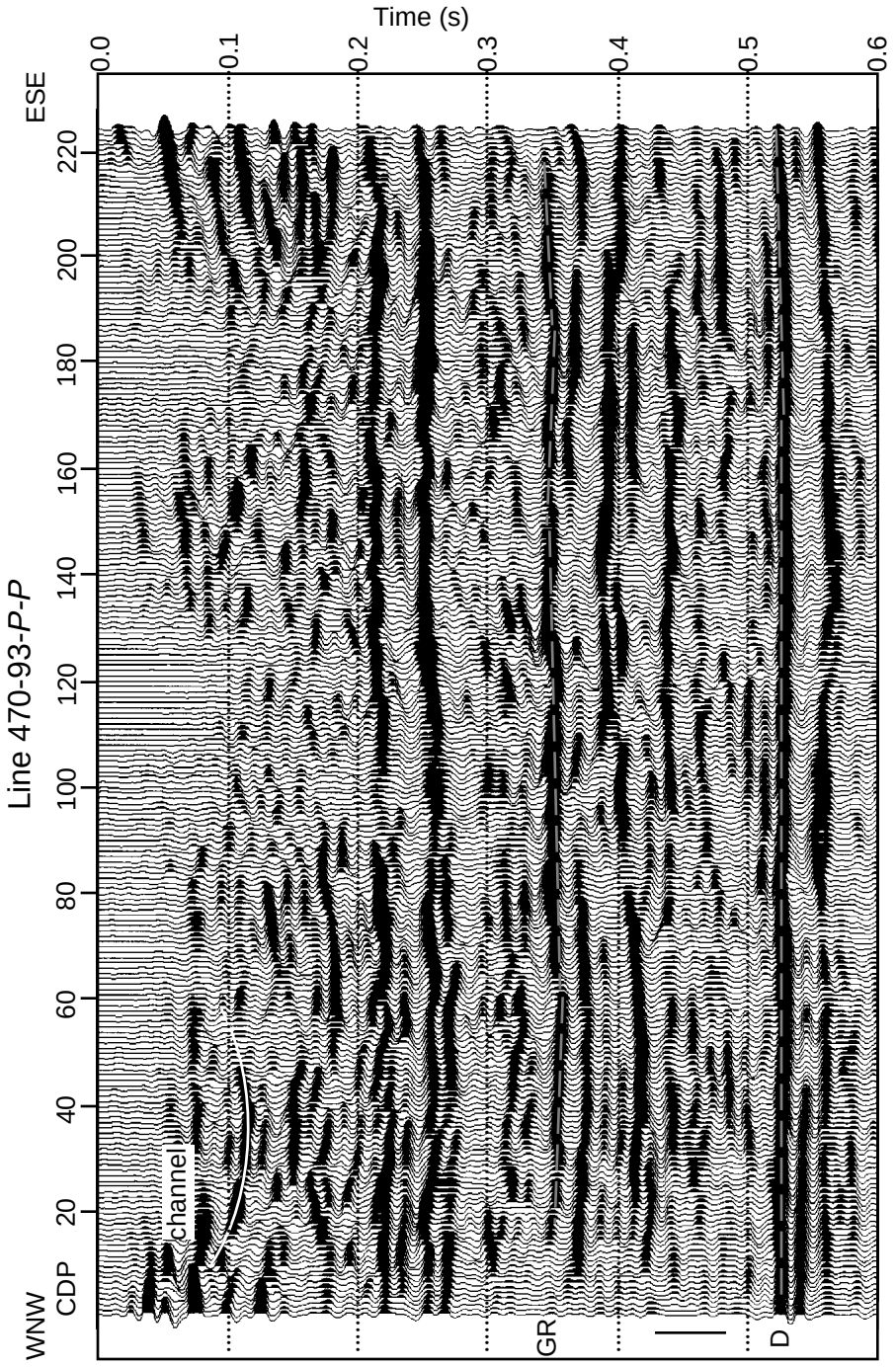

Fig. 11. Interpreted line 470-93-*P-P.*

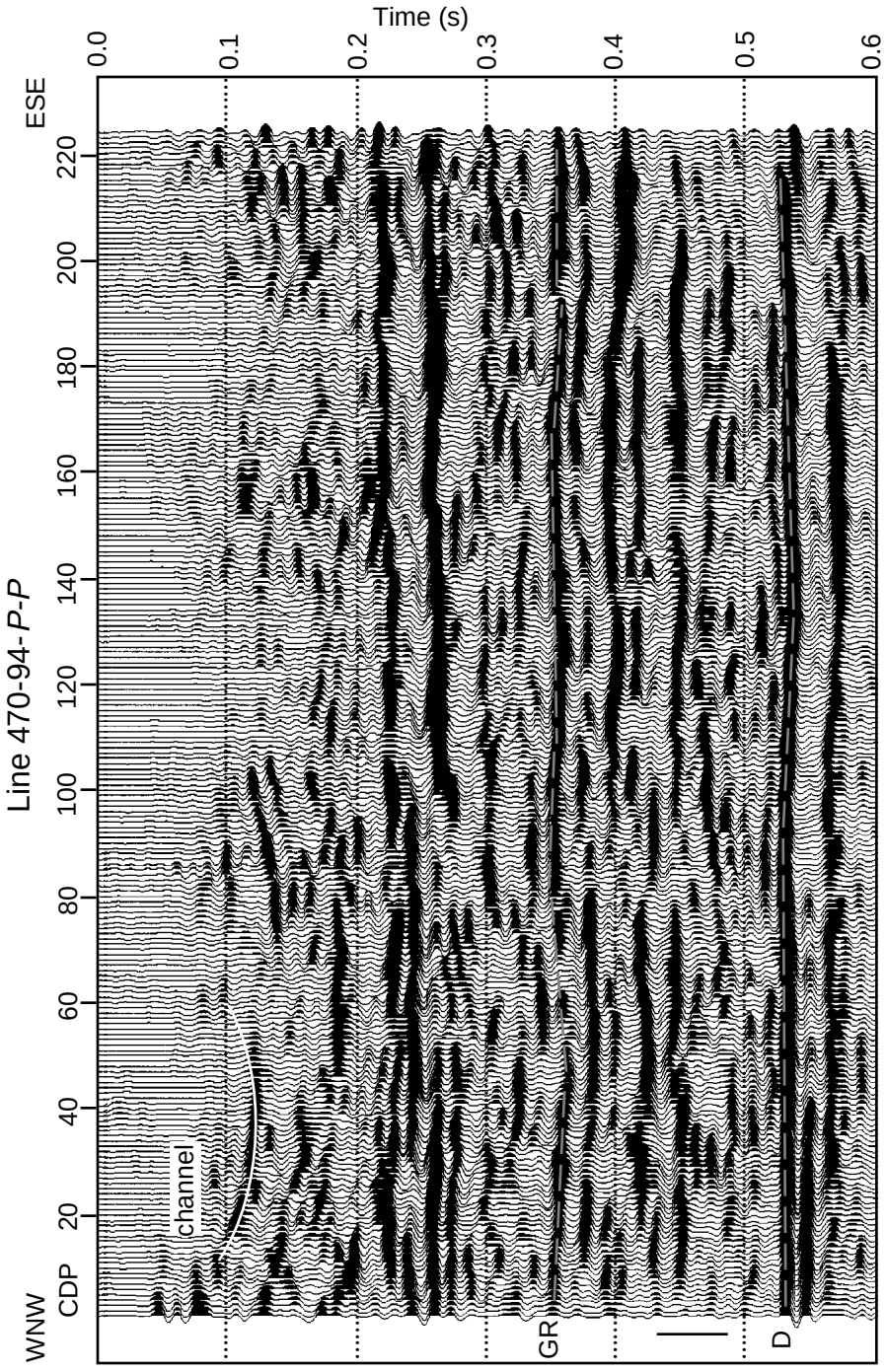

Fig. 12. Interpreted line 470-94-*P-P.*

To estimate the Devonian arrival time on the *P-S* section, an average *Vp/Vs* ratio of 2.4 and the Devonian arrival time of 0.525 s from the *P-P* section were used. This estimated value was calculated to be 0.89 s, so a strong, coherent reflector observed at 0.85 s on the *P-S* section is interpreted to be the Devonian event. The Grand Rapids event is interpreted to be a peak at about 0.58 s as it is the first fairly strong and continuous reflector and the interval transit time between this event and the Devonian (270 ms) is reasonable. A *P-S* synthetic seismogram was created using "SYNTH" and the compressional sonic log from well 27, whose location is shown in Figure 1. The tie between this synthetic seismogram and part of line 470-94-*P-S* is shown in Figure 13. The tie is poor; in particular there are strong events on the seismic section between 0.6 and 0.7 s which do not correlate to the synthetic seismogram. The synthetic seismogram was created using a *P*-wave sonic log acquired a few years earlier than the seismic data, with the *S*-wave sonic log being estimated from this log using a *Vp/Vs* of 2.4. Thus it may not be an accurate model of the *P-S* stacked section.

Figures 14 and 15 show the interpreted *P-S* lines 470-93-*P-S* and 470-94-*P-S*, respectively. The Grand Rapids and Devonian events are annotated on each section and the extent of the reservoir zone is indicated by a bar at the side of the section. On the 1994 line (Figure 15) the Grand Rapids event appears to be of higher amplitude and more continuous than on the 1993 line (Figure 14). Conversely, the top of the Devonian section is of higher amplitude on the 1993 line. The Grand Rapids event appears as a stronger reflection on the *P-S* data than on the *P-P* data. In Figure 9 the relative increase in velocity at the top of this formation is much greater on the *S*-wave sonic log than on the *P*-wave sonic log so the acoustic impedance will be higher.

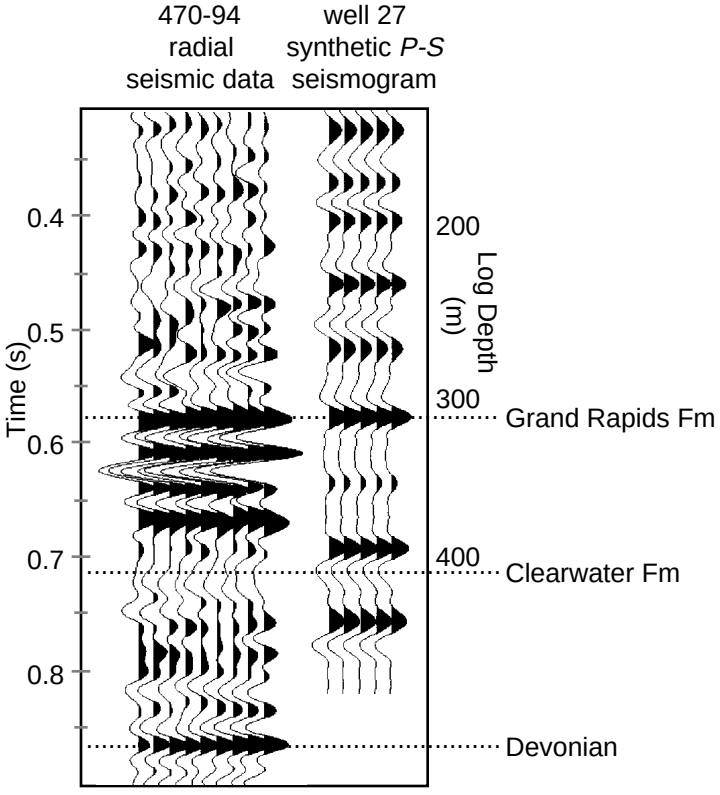

Fig. 13. Tie between *P-S* seismic data and *P-S* synthetic seismogram at well 27.

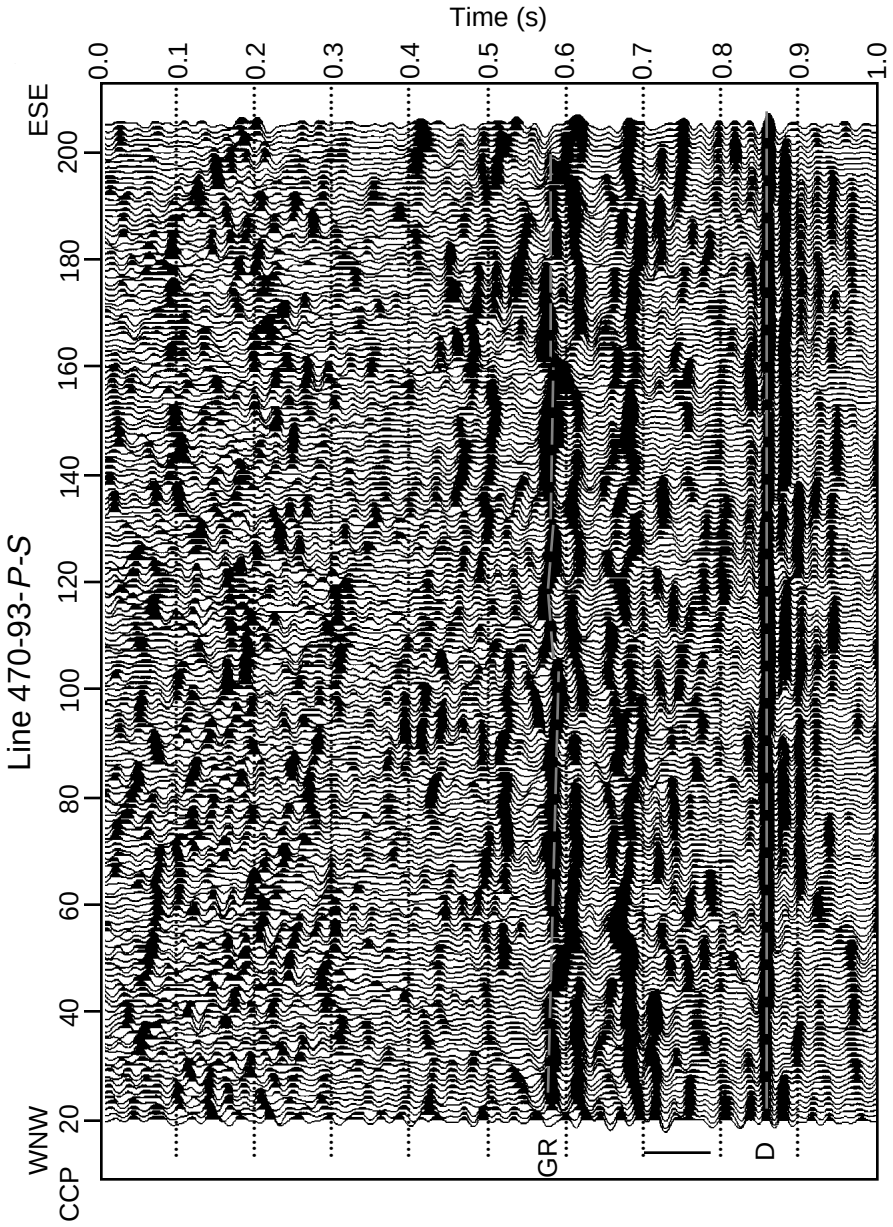

Fig. 14. Interpreted line 470-93-*P-S.*

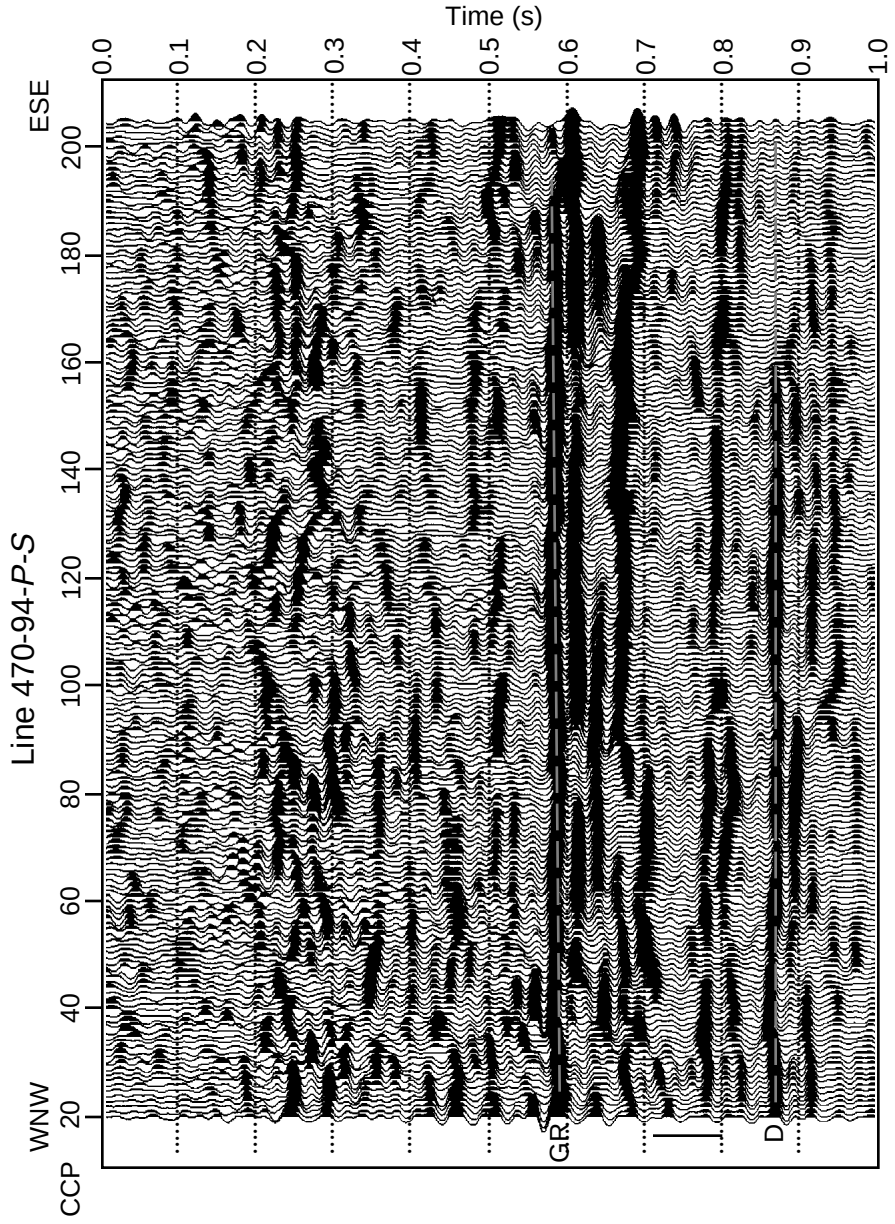

Fig. 15. Interpreted line 470-94-*P-S*.

An example of the tie between the *P-P* and *P-S* sections is shown in Figure 16. The *P-S* section has been displayed at a scale of 0.6 times that of the *P-P* section in order to align events. The *P-P* and *P-S* data are similar in seismic character and apparent frequency. In Figures 17 and 18 the data are windowed on the Grand Rapids to Devonian interval and the *P-S* data are plotted at the same scale as in Figure 16. Amplitude anomalies present on the *P-P* data and absent on the *P-S* data may be attributed to lateral changes in pore fluids.

Vp/Vs analysis

Three pairs of *P-P* and *P-S* sections were loaded onto a workstation and interpreted using SeisX software. The three pairs of line analysed are 470 *P-P* and 470 *P-S*, 468 *P-S* and 469 *P-P*, 472 *P-S* and 471 *P-P*.

The Grand Rapids and Devonian horizons were autopicked on each line after identification of these events on paper sections. On the *P-P* sections little editing of the autopicks was necessary while on the *P-S* sections a little hand-picking was done over areas of questionable correlations. Isochron values were calculated for the Grand Rapids to Devonian interval and *Vp/Vs* determined using equation (1). Results using the Grand Rapids to Devonian were far superior to those using the Clearwater to Devonian interval because the Clearwater pick is inconsistent in this area. Lithology through the Grand Rapids to Devonian interval is assumed to be rather constant here so changes in *Vp/Vs* are expected to reflect changes in *Vp* only.

In Figure 19 are shown the smoothed *Vp/Vs* curves for the Grand Rapids to Devonian interval and the locations of the injection wells for lines 470-93 and 470-94. All these wells were injecting steam into the reservoir at the time of the 1993 seismic data acquisition. The *Vp/Vs* ratios have been smoothed using a five-point weighted median filter. The results from line 470 are displayed because it is considered to be the most reliable line since the stacked data were the highest quality and the picks most dependable. In general there is a good correlation between the locations of the injection wells and low *Vp/Vs* ratios in 1993. The *Vp/Vs* ratios in 1994 are higher over most of the steam injection well locations than in 1993. It is interpreted that the compressional-wave velocities increased here from 1993 to 1994 as the temperature and pore fluid pressure decreased. Some *Vp/Vs* anomalies are present on the 1994 data, particularly over CDPs 130 to 170, and could be caused by gas-saturated zones.

Figure 20 shows the ratio of *Vp/Vs* measured form the 1993 seismic data to that of the 1994 data at each CCP. Values below 1.0 indicate a lower *Vp/Vs* in 1993 (during the steaming cycle) than in 1994 (production) and, in general, are seen over the steamed part of the line and the lowest values correlate to the locations of injection wells. A ratio of 1.0 over the unsteamed part of the line shows that conditions here were more constant from 1993 to 1994 and that the reservoir is still relatively cold.

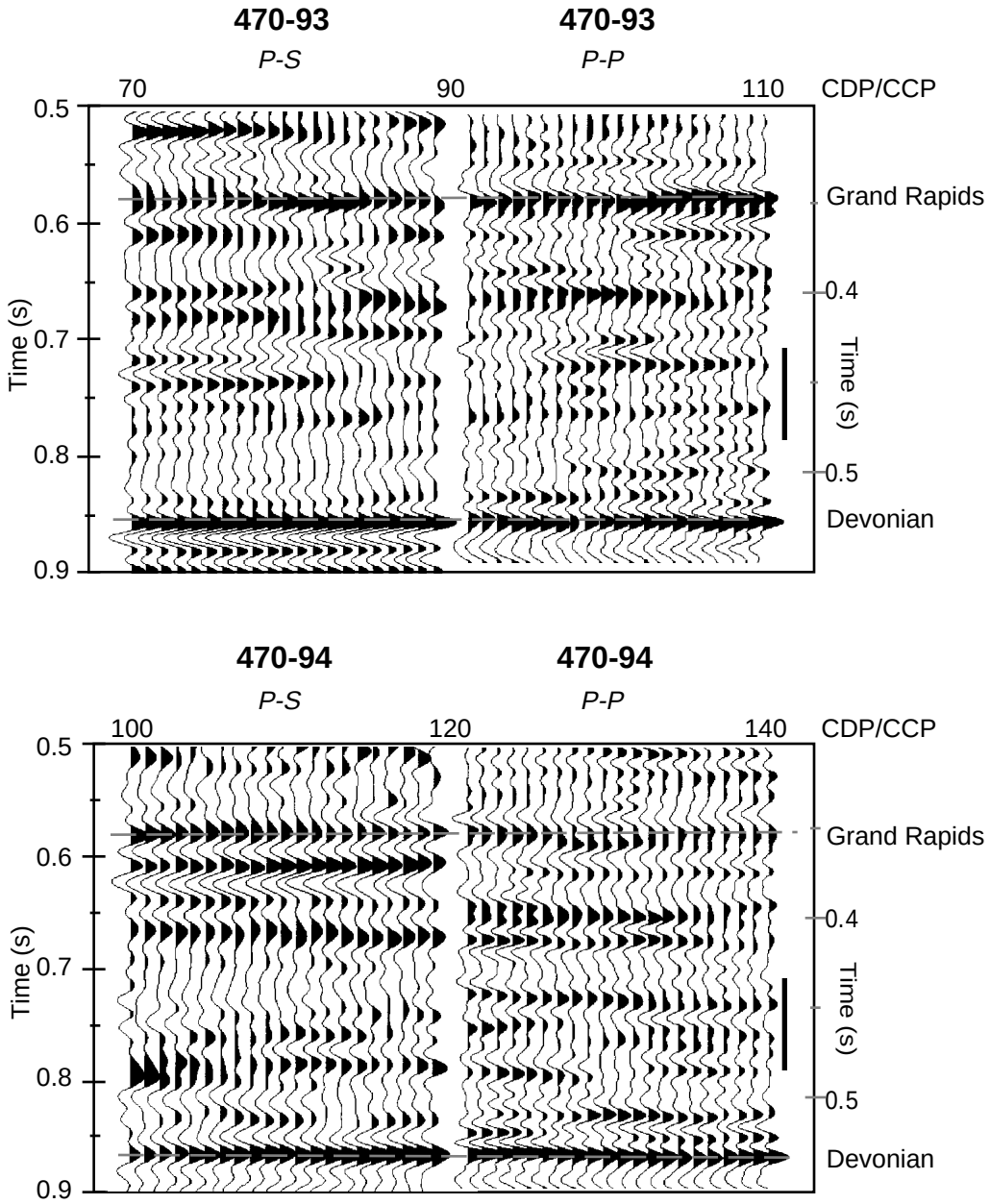

Fig. 16. Examples of ties between *P-P* and *P-S* sections for line 470 from the 1993 and 1994 surveys.

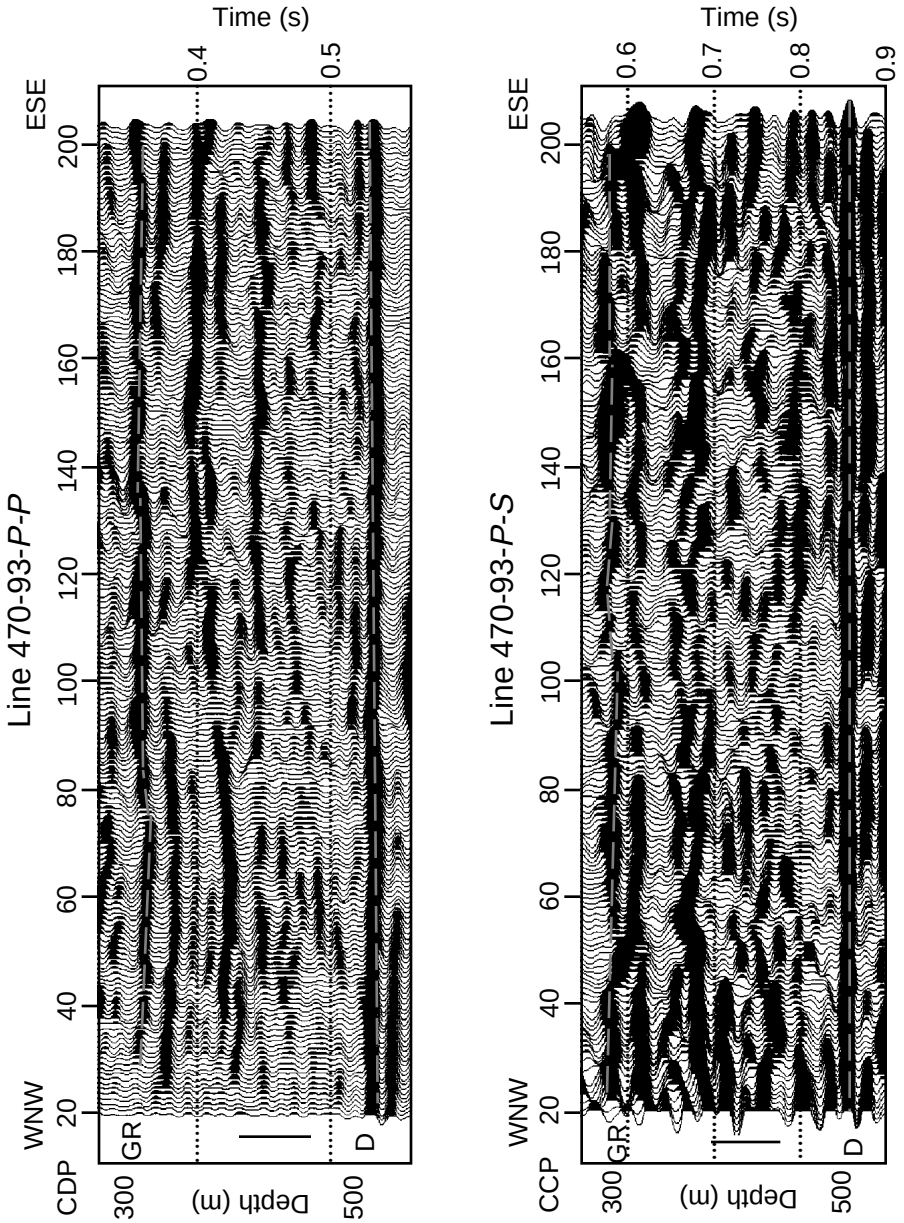

Fig. 17. *P-P* and *P-S* sections for line 470-93 displayed over the same depth interval and windowed on the zone of interest. The reservoir zone is indicated by the bar. GR denotes the top of the Grand Rapids Formation and D the top of the Devonian.

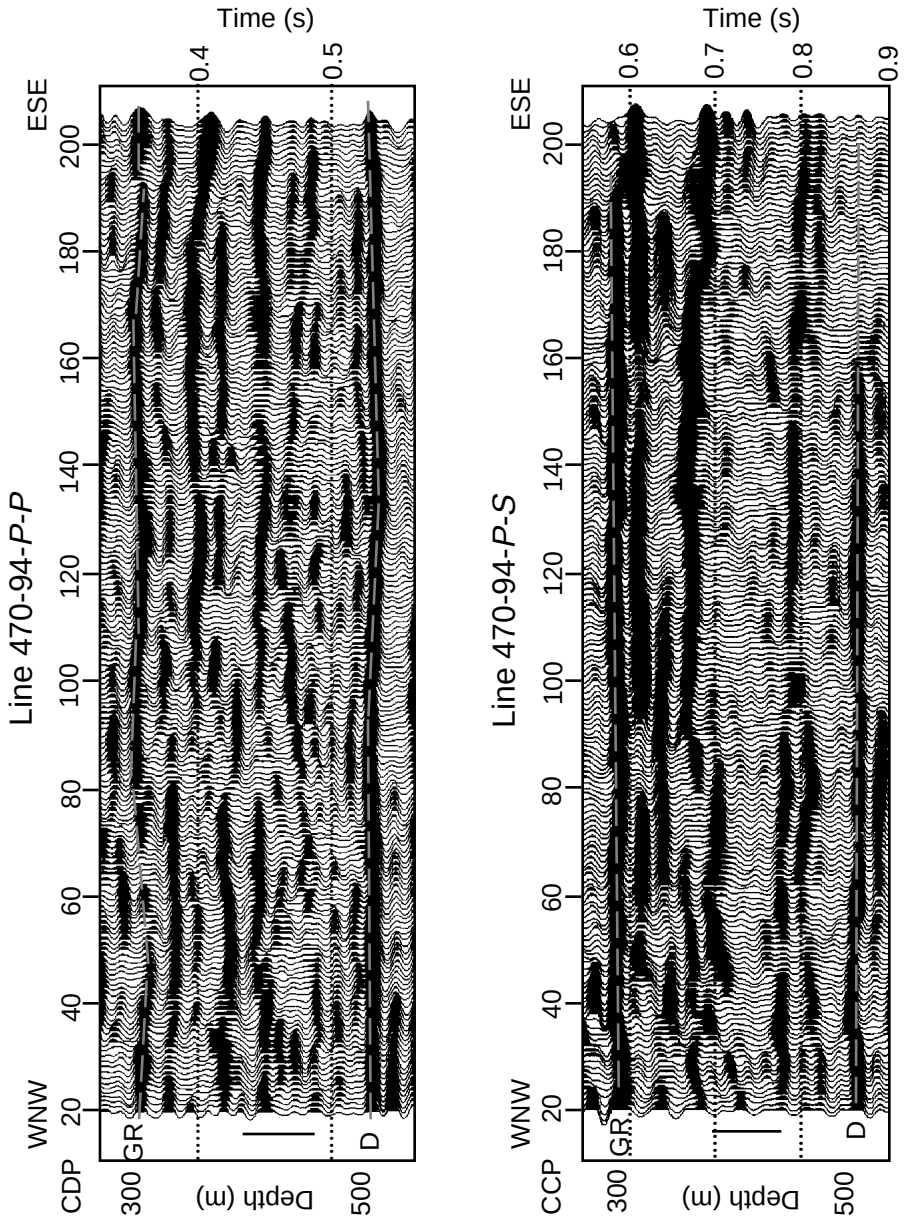

Fig. 18. *P-P* and *P-S* sections for line 470-94 displayed over the same depth interval and windowed on the zone of interest. The reservoir zone is indicated by the bar. GR denotes the top of the Grand Rapids Formation and D the top of the Devonian.

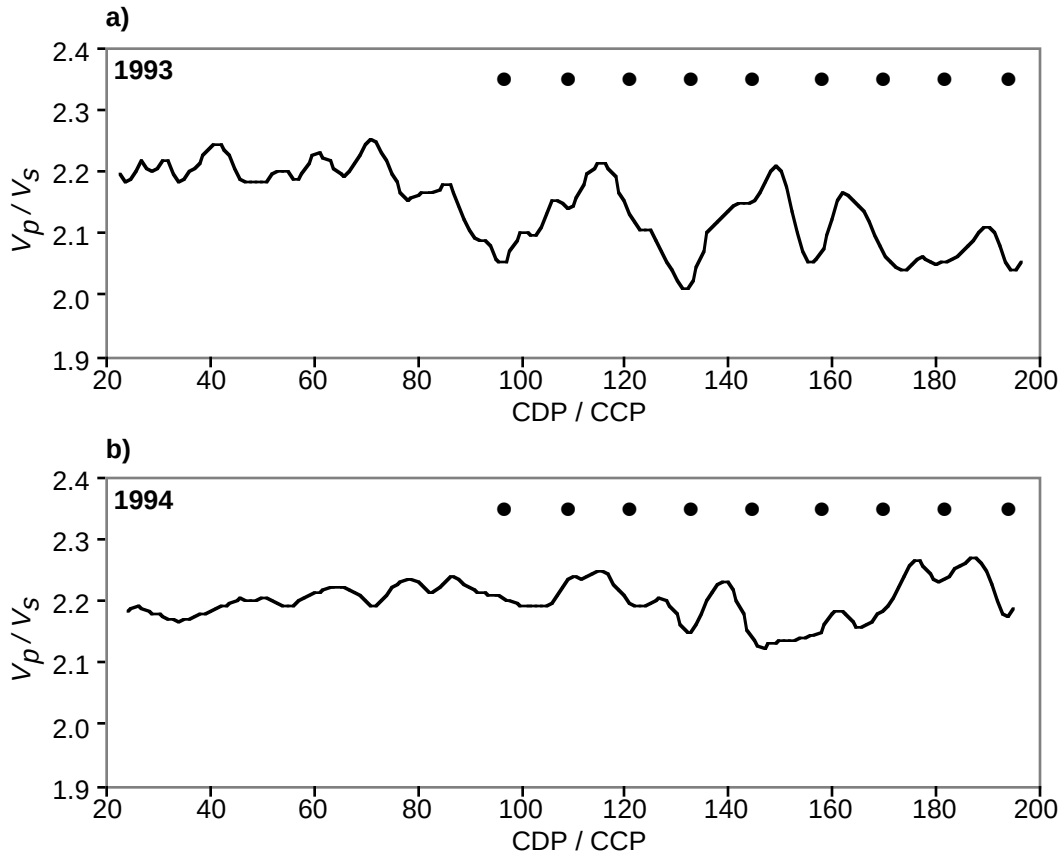

Fig. 19. Smoothed *Vp/Vs* ratios along line 470 for the a) 1993 and b) 1994 surveys. Bullets indicate the locations of steam injection wells.

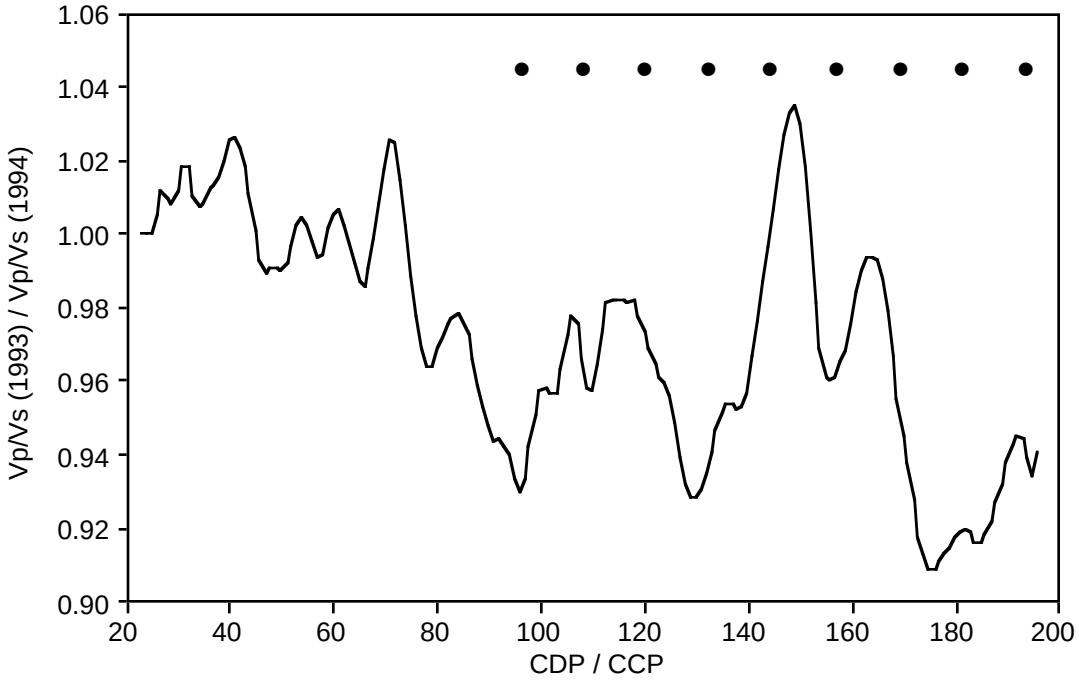

Fig. 20. Ratio of *Vp/Vs* (1993) to *Vp/Vs* (1994).

Using the parameters listed in Table 2, theoretical *Vp/Vs* values over the Grand Rapids to Devonian interval were calculated. *P*-wave velocities for the Grand Rapids and cold Clearwater Formations were obtained from sonic logs while the McMurray Formation *P*-wave velocity was derived from the velocity analyses. *S*-wave velocity in the Grand Rapids Formation was taken from the dipole log run in well 13a. The *S*-wave and *P*-wave velocities in the steamed Clearwater Formation are taken from Eastwood (1993). *S*-wave velocity in the McMurray sands was estimated from equation (2), derived from a crossplot of *Vp* versus *Vs* in sandstones (Castagna et al., 1993).

$$Vs = 0.8042Vp - 0.8559 \text{ (km/s)} \qquad (2)$$

Table 2. Parameters used to determine *Vp/Vs* in the cold reservoir

Event	**Depth (m)**	***Vp***	***Vs***	***Vp/Vs***
Grand Rapids	315	2420	1000	2.42
Clearwater	415	2350 (cold) 1600 (hot)	1185	1.98 1.35
McMurray	470	2700	1315	2.05
Devonian	530			

Figure 21 shows the theoretical *Vp/Vs* values obtained using these parameters for a steamed zone ranging in thickness up to 40 m, which is the maximum thickness of clean homogeneous reservoir in this locality. Plotted also are curves obtained by substituting steamed zone interval velocities of 1800 m/s and 2000 m/s. It can be seen from this plot that relating a particular value of *Vp/Vs* to a unique thickness of steamed zone is not possible without knowledge of the temperature conditions. However, a theoretical lower limit of 2.022 for the heated reservoir and a value of 2.208 for the cold reservoir are calculated. The rms value for *Vp/Vs* in the cold part of the reservoir as measured from the 1993 seismic data is 2.2 and the lowest measured value is 2.012. These values are in excellent agreement with the theoretical limits.

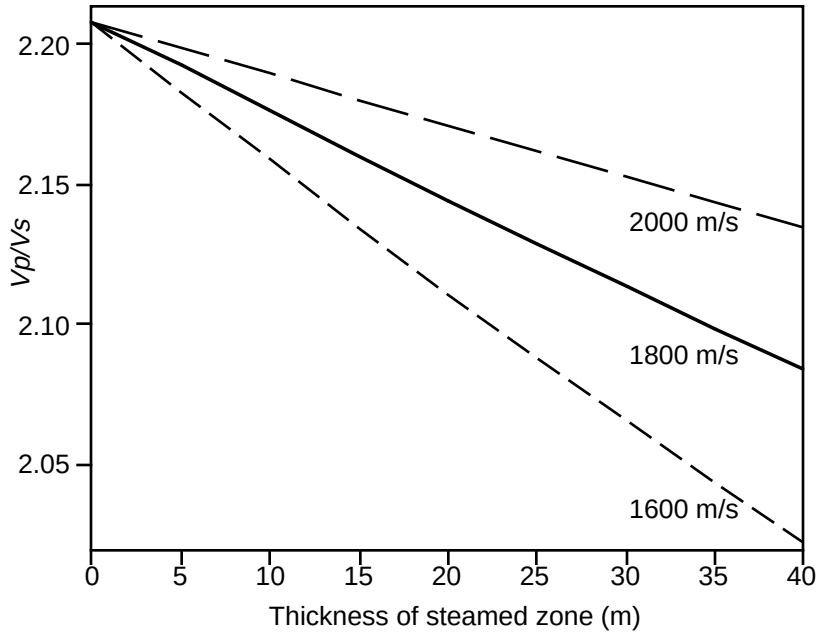

Fig. 21. Plot of thickness of steamed zone versus theoretical *Vp/Vs* for steamed zone interval velocities of 1600, 1800 and 2000 m/s.

CONCLUSIONS

Two experimental time-lapse converted-wave surveys were recorded during the acquisition of 3-D seismic surveys as part of a reservoir monitoring programme at an EOR project in Cold Lake, Alberta. Determination of the very large receiver statics to be applied to the *P-S* data was an important factor in the production of an interpretable stacked section. Other significant processing factors were the determination of stacking velocities and the application of spiking deconvolution after NMO-corrections. Burial of the 3-C geophones may help to decrease the very large receiver statics and increase the signal to noise ratio.

The final, migrated sections were interpreted on a workstation. *Vp/Vs* values were calculated for each pair of *P-P* and *P-S* lines from the interval transit times of the Grand Rapids to Devonian section. Over the part of the lines away from the steam injection wells the measured rms *Vp/Vs* was 2.2, which is in good agreement with the theoretical value of 2.208 for the cold reservoir. For the survey shot in 1993, during the steam injection cycle, low *Vp/Vs* values correlated well with the locations of the steam injection wells and the minimum value measured was 2.012, which agreed with the theoretical minimum value of 2.022. For the production survey in 1994, the V_P/V_S values were generally higher over the well locations. The preliminary interpretation results give encouragment that acquisition of converted-wave surveys can offer information complementary to that obtained from 3-D surveys in this study area.

ACKNOWLEDGEMENTS

The authors would like to acknowledge Imperial Oil Resources Ltd., especially Dr. John Eastwood, for their cooperation in this project.

REFERENCES

Castagna, J. P., Batzle, M. L. and Kan, T. K., 1993, Rock physics - the link between rock properties and AVO response *in* Castagna, J. P. and Backus, M. M., Eds., Offset dependent reflectivity-theory and practice of AVO analysis: Soc. Expl. Geophys.

Eastwood, J., 1993, Temperature-dependent propagation of *P*- and *S*-waves in Cold Lake oil sands: Comparison of theory and experiment: Geophysics, **58**, 863-872.

Harrison, M. P. and Stewart, R. R., 1993, Poststack migration of *P*-*S* seismic data: Geophysics, **58**, 1127-1135.

Isaac, J. H. and Lawton, D. C., 1994, 3-D and 3-C seismic data analysis at Cold Lake, Alberta: CREWES Research Report, Volume **6**, 18.1-18.22.

Iverson, W. P., Fahmy, B. A. and Smithson, S. B., 1989, V_pV_S from mode-converted *P*-*S* reflections: Geophysics, **54**, 843-852.

Lane, M. C. and Lawton, D. C., 1993, 3D converted wave asymptotic binning: CREWES Research Report, Volume **5**, 29.1 -29.5.

Tosaya, C., Nur, A., Vo-Thanh, D. and Da Prat, G., 1987, Laboratory seismic methods for remote monitoring of thermal EOR: S.P.E. Res. Eng., **2**, 235-242.

Wang, Z. and Nur, A., 1988a, Effect of temperature on wave velocities in sands and sandstones with heavy hydrocarbons: S.P.E. Res. Eng., **3,** 158-164.

Wang, Z. and Nur, A., 1988b, Seismic velocities in heavy oil and tar sands: The basis for reservoir monitoring: Proc. of the 4th internat. conf. on heavy crude and tar sands, **4,** 601-611.